CHARACTERISATION OF CONCRETE FROM THE RUPNIK MILITARY LINE

KARAKTERIZACIJA BETONOV RUPNIKOVE LINIJE

Tilen Turk[1], Petra Štukovnik[1], Marjan Marinšek[2], Violeta Bokan Bosiljkov[1*]

[1]University of Ljubljana, Faculty of Civil and Geodetic Engineering, Jamova cesta 2, 1000 Ljubljana, Slovenia
[2]University of Ljubljana, Faculty of Chemistry and Chemical Technology, Večna pot 113, 1000 Ljubljana, Slovenia

The Rupnik military line was established in about 1935 in the Kingdom of Yugoslavia as a defence system against the Kingdom of Italy. It consists of more than 4000 reinforced concrete military bunkers positioned on the eastern part of the Rapallo border, varying in size and purpose, and was a top-secret project at the time. Different non-destructive and non-invasive techniques were used to characterise the selected bunkers and carefully conceived concrete samples to gain an insight into the concrete technology used to build these historic military infrastructures. The results of the non-destructive techniques were further compared to those of destructive techniques for a given property. It was established that very different concrete compositions were used to build the bunkers, and an extensive dispersion of the properties was confirmed for each composition. The average compressive strength of the Schmidt hammer for a given position is an acceptable estimate of the actual compressive strength of concrete without destructive intervention into a bunker. It also enables an estimation of the secant modulus of elasticity using the ModelCode2010 approach. Cylinders drilled from a bunker provided additional information about the concrete petrography, its physical and mechanical properties and the durability of reinforced concrete.

Keywords: historic concrete, military bunker, non-destructive testing, ultrasound, Schmidt hammer, optical microscopy, image analysis

Rupnikova linija je linija vojaških utrdb, ki je bila v času vladavine Jugoslavije zgrajena kot obrambni sistem pred vdorom vladavine Italije, okrog leta 1935. Sestavlja jo več kot 4000 armiranobetonskih vojaških utrdb vzhodno od rapalske meje, različnih velikosti in namembnosti. Zato so natančne mikrolokacije bunkerjev in tehnologijo gradnje poznali le redki. Za karakterizacijo izbranih bunkerjev so bile uporabljene različne neporušne in neinvazivne tehnike ter skrbno odvzeti betonski valji, da bi dobili vpogled v tehnologijo, uporabljeno za gradnjo teh zgodovinskih vojaških utrdb. Rezultate neporušnih tehnik smo primerjali z rezultati porušnih tehnik za posamezno lastnost. Ugotovili smo, da so bile za gradnjo bunkerjev uporabljene zelo različne sestave betona, za vsako sestavo pa je bila potrjena velika razpršenost lastnosti. Povprečna tlačna trdnost, ocenjena s Schmidtovim kladivom za posamezno pozicijo, predstavlja sprejemljivo oceno dejanske tlačne trdnosti betona brez posega v konstrukcijo. Omogoča tudi oceno stabiliziranega sekantnega modula elastičnosti, z uporabo pristopa ModelCode2010. Valji, izvrtani iz bunkerja, so omogočili pridobitev dodatnih informacij o petrografiji betona, njegovih fizikalnih in mehanskih lastnostih ter trajnosti armiranega betona.

Ključne beside: zgodovinski beton, vojaški bunker, neporušne preiskave, ultrazvok, sklerometer, optična mikroskopija, analiza slik

1 INTRODUCTION

The Rupnik military line, located in the western part of Slovenia, is a fortification line built at the time of the Kingdom of Yugoslavia, along the Rapallo Border between the Kingdom of Yugoslavia and the Kingdom of Italy, established with the bilateral agreement signed on November 12, 1920.[1] The Yugoslav military leadership considered the Kingdom of Italy to be the main threat to the freedom of the Kingdom of Yugoslavia. Therefore, they decided to build two fortification systems: a lowland fortification system and a ridgetop fortification system, positioned to the eastern side of the Rapallo Border, following the French building model used in the Maginot line.[2] In the lowland fortification systems, primarily machine-gun nests, light-artillery bunkers and obstacle systems were built. The ridgetop positions were used to pro-

tect the lowland system in the case of heavy enemy attacks, so many changes to the landscape (forestation and deforestation) were also made to ensure the blending of the bunkers with nature. Reinforced concrete bunkers were positioned strategically to ensure proper border protection.[3]

The military bunkers are built of reinforced concrete. The concrete walls are often rendered with a unique cementitious mixture to protect the concrete from environmental factors, such as rain, snow, freezing/thawing, etc., and to blend the bunkers with nature (**Figure 1 left**). Inside the bunkers, there is often evidence of poor compaction, indicating that the fresh concrete had poor filling capacity (**Figure 1 right**). When these defects were extensive, they were repaired with cement render (external surfaces) or plaster (internal surfaces).

Determining the mechanical properties of heritage materials to design compatible repair or strengthening materials is often difficult because only a limited number

*Corresponding author's e-mail:
Violeta.Bokan-Bosiljkov@fgg.uni-lj.si (Violeta Bokan Bosiljkov)

Figure 1: Ridgetop bunker perfectly blended with nature (left) and poor concrete compaction due to low workability (right)

of samples can be taken from historical structures. Thus, various non-destructive testing methods are used for the *in situ* characterisation of particular properties. Concrete condition and building technology can be determined in part by the ultrasonic waves test method, which measures the transmission times of longitudinal and shear waves. Dynamic *E*-modulus, Poisson's ratio, and shear *G*-modulus can be straightforwardly calculated when the ultrasound transmission times are known.[4] On the other hand, compressive strength can be non-destructively estimated using a Schmidt hammer.

Non-destructive techniques are extremely useful tools for the *in-situ* characterisation of concrete and its quality control, which is reflected in the available standard test methods in this area.[5,6] However, historic reinforced concrete structures very often show a lack of homogeneity and a high concentration of defects compared to modern concrete structures. This work, therefore, focuses on the characterisation of 80-year-old concrete samples taken from two bunkers of the Rupnik military line, using ultrasonic wave and Schmidt hammer test methods. The results of the non-destructive testing are compared with those of the conventional destructive testing performed on concrete cylinders taken from the bunkers.

The measured mechanical properties are further substantiated by a petrographic analysis of concrete specimens, in which aggregate type, microstructure changes and cement type were determined.

2 EXPERIMENTAL PART

2.1 Sampling

Due to the requirements of the competent authority for minimal interventions into the reinforced concrete elements of the bunkers, only three concrete cores per bunker were drilled in the first phase of the study. The concrete cores were carefully taken from a selected lowland bunker (group A1) and a ridgetop bunker (group C1). Before drilling, the two bunkers were scanned with the Hilti Ferroscan PS 300 device to determine the loca-

tion of the steel reinforcement and thus avoid drilling through the reinforcement, if possible. On selected drilling positions, the rebound index was determined first by using the Schmidt rebound hammer (Proceq) and following the standard procedure.[6] The cores were taken from inside the bunkers, according to the EN 12504-1 standard.[7] The Hilti diamond coring machine with a core drill bit of 100 mm was used to obtain concrete cores with a diameter of 94 mm and length of 200–300 mm. The drilled holes were immediately filled by repair mixture compatible with the original concrete.

2.2 Preparation of samples

The two groups of concrete samples (A1 and C1) are cylinders with a diameter of 94 mm and a height of 92–95 mm. The samples were obtained by cutting the concrete cores taken from the bunkers. If a steel bar was present in the core, this part of the core was cut off before sample preparation. The cut-off discs were used to make thin sections and to determine the aggregate-to-binder ratio. The cylinders were stored under laboratory conditions at a humidity of about 50 % until testing. Prior to testing, the ends of the samples were ground to achieve the tolerances of flatness and perpendicularity, according to EN 12390-1.[8]

2.3 Estimation of aggregate-to-binder ratio

The aggregate-to-binder-to-pore ratio was estimated by image analysis of the cross-sectional area of the cylinders. The total area of the aggregate grains and the total area of the pores in the cross-section were divided by the cross-sectional area (stereological theory). A Hirox KH-3000 VD scanning optical microscope was used for the surface imaging.

2.4 Optical microscopy

Polarised transmission optical microscopy was performed on thin sections of the samples. For mineralogi-

cal characterisation of the aggregate the samples were coloured with the alizarine red colourant. Microscope images were taken at 50× magnification in PTT mode with a Zeiss LSM-700 microscope (Co-Namaste).

2.5 Dynamic elastic parameters and density

For measuring the transmission time of longitudinal ultrasonic waves (P-waves) and ultrasonic shear waves (S-waves), the Proceq Pundit PL-200 device was used, with an operating frequency range of 20 kHz to 500 kHz. With the ultrasonic method, the dynamic elastic modulus, dynamic Poisson's ratio and dynamic shear modulus were determined using 250-MHz Olympus shear-wave transducers. Modern concrete cast in structural elements is a homogeneous, isotropic elastic material; therefore, the equations for calculating the dynamic elastic parameters of such materials can be used (Equation (1) to (3)).[9] The equations are based on the transmission velocity of ultrasonic P- and S-waves and the bulk density of the material:

$$\nu_d = \frac{V_p^2 - 2V_s^2}{2(V_p^2 - V_s^2)} \quad (1)$$

$$E_d = V_p^2 \rho \frac{(1+\nu_d)(1-2\nu_d)}{(1-\nu_d)} = 2V_s^2 \rho(1+2\nu_d) \quad (2)$$

$$G_d = \frac{E_d}{2+2\nu_d} = V_p^2 \rho \quad (3)$$

where ν_d stands for the dynamic Poisson's ratio, V_P is the transmission velocity of ultrasonic P-waves, V_S is the transmission velocity of ultrasonic S-waves, E_d is the dynamic elastic modulus, G_d the dynamic shear modulus and ρ is the concrete density.

The concrete density was determined for each sample as the quotient of its mass and volume.

2.6 Compressive strength and static modulus of elasticity

The static modulus of elasticity (E-modulus) was estimated using the modified EN 12390-13 standard procedure.[10] Modifications used are the length-to-diameter ratio of the specimen, which is about 1, instead of 2 to 4, and the estimation of concrete compressive strength, based on our own expertise, in order to determine the upper stress (1/3 of the compressive strength) to which the load was increased during the test. These two modifications were necessary due to the limited number of specimens that could be taken from the concrete cores. The strain measuring instruments were two deformeters with a gauge length of 50 mm.

Method A of the EN 12390-13 standard was applied in order to determine the initial (E_{sI-in}) and stabilised ($E_{sIII-dec}$) secant (static) E-modulus, with one modification – stabilised secant E-modulus was determined in the third unloading cycle (denotation III-dec), instead of the third loading cycle, according to the COST TU1404 researchers' proposal.[4] The E-moduli were calculated with an upper-stress value of 16 MPa and a lower-stress value of 6 MPa, and the corresponding deformations.

The compressive strength was determined only after the static E-modulus test had been completed, using the EN 12390-3 standard procedure.[11] The compressive strength determined on a cylinder with a diameter-to-length ratio of about one is considered as the cube compressive strength. The 100/100 mm cylinder compressive strength is about 7 % lower than the 150 mm cube compressive strength and can be used to determine a concrete's compressive strength class.
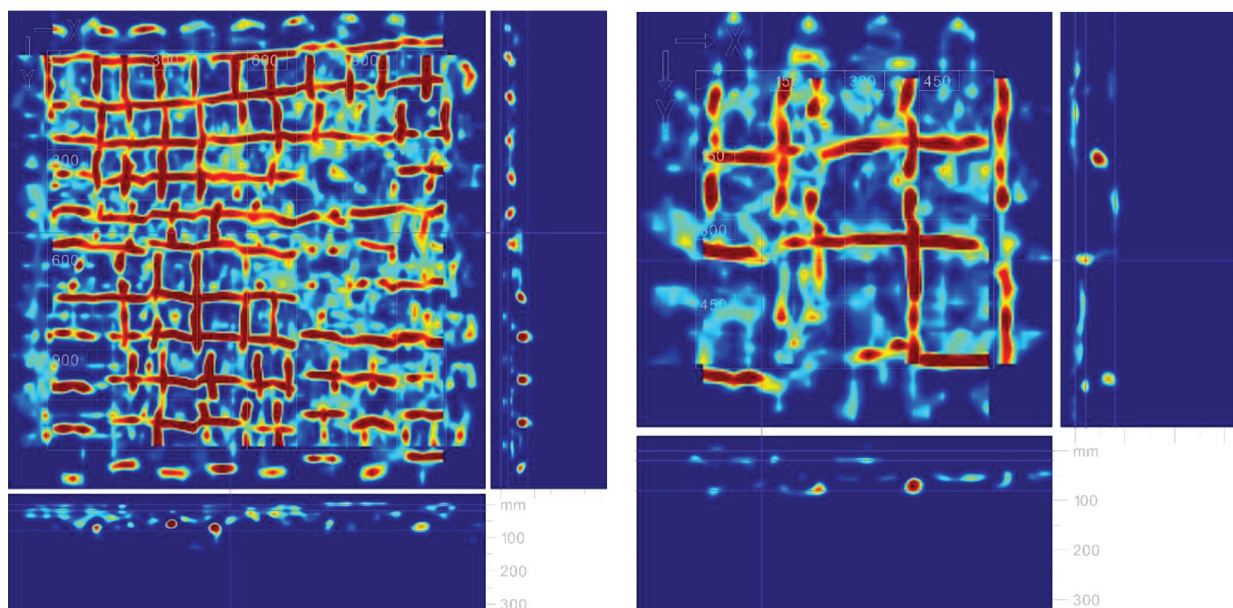

Figure 2: Image of steel reinforcement scanned with Hilti PS-1000 for the lowland (left) and the ridgetop (right) bunker

3 RESULTS

3.1 Visual appearance of steel reinforcement and concrete cores

Figure 2 presents images of steel reinforcement in the lowland and the ridgetop bunker. From the images we can conclude that the steel mesh sheets were used to reinforce the concrete bunkers and that at least two sheets were used in the inner part of the concrete wall where they are positioned at a depth between 0 mm and 80 mm. The smaller lowland bunker was reinforced more heavily than the ridgetop bunker, since the clear distance between the steel bars is between 100 mm and 150 mm for the former and about 200 mm for the latter.

Based on the steel-reinforcement images, the optimal positions of the Hilti coring assembly were determined (**Figure 3 left**). However, for the lowland bunker the acquired cores contained parts of steel bar (**Figure 3 right**), which can be attributed to the small opening of the steel mesh and the overlap of the two layers. These steel-bar segments revealed the good condition of the steel reinforcement in the bunker, even after 80 years. There is no sign of steel corrosion, despite the presence of voids between the concrete and the surface of the steel bars. These voids are the consequence of inefficient concrete compaction during construction works.

The visual appearance of the concrete cores (**Figure 3 right**) shows an efficient skeleton of aggregate grains that predominantly occupy the concrete volume, and a just large enough content of hydrated cement paste to bind the grains into the concrete composite.

3.2 Aggregate shape and aggregate-to-binder ratio

The aggregate-to-binder-to-pore ratio for samples A1, taken from the lowland bunker, was estimated to be around 78 : 20 : 2, while for samples C1, taken from the ridgetop bunker, it was 47 : 51 : 2. The aggregate grains are predominantly angular, similar to today's crushed natural aggregate grains. However, much higher volumes of elongated particles were observed in the concrete samples (**Figure 3 right**), compared to today's concrete compositions. It is not yet clear how the angular grains for concrete production were obtained. According to the oral information given by a local resident, the stone grains separated from the rocks of the nearby mountains

Figure 3: Coring of the concrete samples (left) and concrete cores taken from the lowland bunker (right)
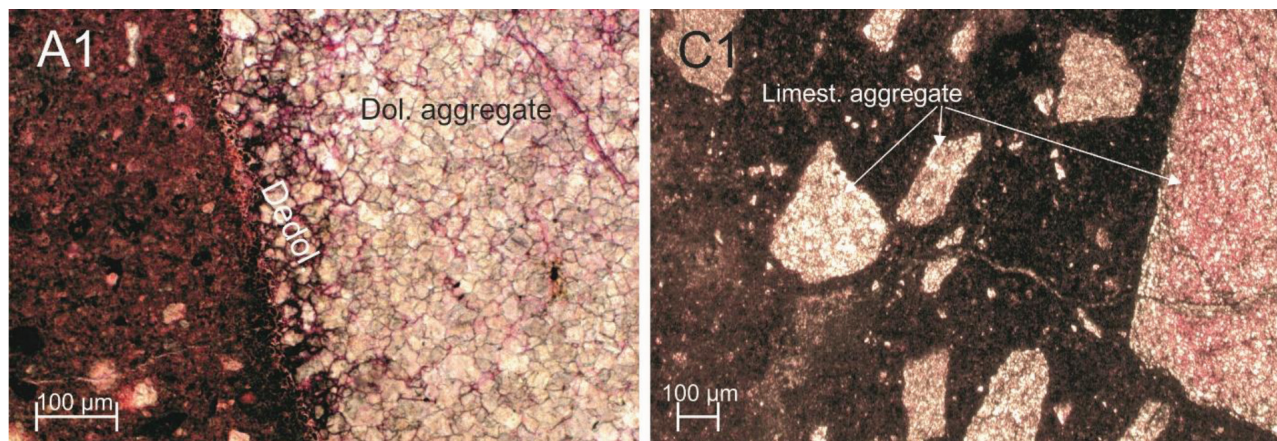

Figure 4: Petrography of samples A1 and C1 under polarised transmission optical microscope

(due to erosion) were transported into the valleys by torrents and were deliberately used as a source of aggregate. Engineering solutions that enable the grain deposition were applied to collect the aggregate for the concrete. In addition, there is information that the army has also opened some quarries to produce aggregate for the concrete.[3]

3.3 Optical microscopy

Petrographic analyses of the thin sections showed that concrete composition A1 was prepared using dolomite aggregate (**Figure 4 left**), and concrete composition C1 with limestone aggregate (**Figure 4 right**). Binder used for the two concrete compositions was most probably a mixture of Portland cement clinker and blast furnace slag (**Figure 4**). Moreover, the presence of dedolomitization and secondary calcite formation is evident from the thin section A1, and the microcracks are filled with secondary products in both compositions.

3.4 Concrete density, compressive strength and elastic properties

The main properties of hardened concrete specimens A1 and C1 are given in **Table 1**. As reference values, the same properties of modern concrete M1 are provided. River gravel and sand with predominantly carbonate grains and a grain density of about 2750 kg/m³ occupy 75 % of the M1 concrete volume. From the results in **Table 1** it is evident that concrete specimens A1 have a lower density, compared to the concrete specimens C1, despite the higher density of the dolomite aggregate (values from 2810–2840 kg/m³), compared to the limestone aggregate (values of 2660–2760 kg/m³).[12] The characteristic compressive strength of concrete A1 is about 25 MPa (average value – 2·standard deviation), and for concrete C1 it is 30 MPa. The repeatability of the com-

pressive-strength results for concrete compositions A1 and C1 is low, with standard deviations of 11 MPa and 15 MPa, respectively. For the modern concrete compositions, the standard deviation of compressive strength is 3–6 MPa, which is confirmed by the M1 test results.

Estimation of the concrete's compressive strength using the Schmidt hammer average value gave realistic results for the cylinder's compressive strength (0.8 cube compressive strength) for all samples but A1-1, where the estimated compressive strength was extremely low.

The modulus of elasticity is also higher for composition C1, although its aggregate volume is much lower (about 50 %) than for concrete A1 (about 80 %). This is true for the dynamic (Young's) and static moduli of elasticity.

However, there is a large difference between the initial and stabilised secant E-moduli, which is not consistent with modern concrete properties, where the differences are small. **Figure 5** illustrates typical stress-strain diagrams used to determine the static E-modulus of sam-
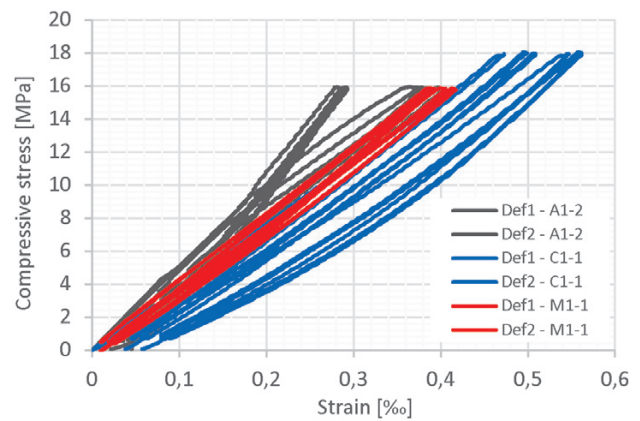
Figure 5: Compressive stress-strain diagrams for the determination of static E-modulus

Table 1: Properties of hardened concrete

	$\rho/(kg/m^3)$	f_c/MPa	E_d/GPa	ν_d	G_d/GPa	$E_{sI\text{-}in}/GPa$	$E_{sIII\text{-}dec}/GPa$	$f_{c\text{-}Schmidt}/MPa$
A1-1	2284	46	42	0.32	16	23	32	22 ± 7.5
A1-2	2381	58	54	0.27	21	55	53	46 ± 13.5
A1-3	2260	37	40	0.30	15	26	32	32.5 ± 13.3
A1aver	2310	47	46	0.30	18	35	39	34
STD	60	11	8	0.03	3	18	12	12
C1-1	2483	76	55	0.33	21	38	43	56.5 ± 15.3
C1-2	2400	46	45	0.35	17	25	32	47.5 ± 27.8
C1-3	2472	59	47	0.30	18	60	63	51 ± 17.8
C1aver	2450	60	49	0.33	19	41	46	52
STD	50	15	5	0.03	2	18	16	5
M1-1	2426	58	51	0.27	20	37	37	–
M1-2	2435	60	54	0.26	21	39	40	–
M1-3	2448	63	58	0.25	23	40	41	–
M1aver	2440	60	54	0.26	21	39	39	–
STD	10	3	4	0.01	2	2	2	–

ρ – concrete density, f_c – compressive strength, E_d – dynamic elastic modulus, ν_d – dynamic Poisson's ratio, G_d – dynamic shear modulus, $E_{sI\text{-}in}$ – initial and $E_{sIII\text{-}dec}$ – stabilised secant (static) E modulus, $f_{c\text{-}Schmidt}$ – compressive strength estimation with Schmidt hammer

ples M1-1 (f_c = 58 MPa, E_{sI-in} = 37 GPa, $E_{sIII-dec}$ = 37 GPa), A1-2 (f_c = 58 MPa) and C1-1 (E_{sI-in} = 38 GPa, $E_{sIII-dec}$ = 43 GPa). Samples M1-1 and C1-1 have almost the same E_{sI-in}, with the compressive strength of C1-1 about 38 % higher. For the historic sample C1-1, relatively large residual deformations were measured after the last loading/unloading cycle. Sample A1-2, on the other hand, has approximately the same compressive strength as M1-1, but its average static E-modulus and residual deformations are considerably higher.

Poisson's ratio v_d of concrete samples A1 and C1 is high (0.3 ± 0.03 and 0.33 ± 0.03, respectively) when compared to the modern concrete values, which are around 0.25 for mature concrete. The higher v_d of samples C1 is due to the higher hydrated cement paste content. The Poisson's ratio of the hydrated cement paste can be higher by about 0.05, compared to the concrete in which the same cement paste glues the aggregate grains together.[9]

The static E-modulus is often estimated using different regression equations, from compressive strength or dynamic E-modulus. By using the approach given in ModelCode 2010[13] (Equation (4)), we first calculated the static E-moduli from the compressive strengths of the samples A1, C1 and M1. Next, we estimated the static E-modulus from the dynamic E-modulus, by using Equation (5), for the three concrete compositions. The estimated static E-moduli and parameters of Equations (4) and (5) are given in **Table 2**.

$$E_{s-est-MC} = E_{c0} \cdot \alpha_E \left(\frac{f_c}{10} \right)^{1/3} \qquad (4)$$

$$E_{s-est-E_d} = a \cdot E_d^b \qquad (5)$$

$E_{s-est-MC}$ stands for static E-modulus estimated by ModelCode2010, and $E_{c0} \cdot \alpha_E$ presents the effect of the aggregate type on the E-modulus. $E_{s-est-Ed}$ stands for the static E-modulus estimated from the dynamic modulus E_d, calculated from the ultrasonic test results.

Table 2: Parameters of regression equations and estimated static E-modulus

	$E_{c0}\alpha_E$/MPa	$E_{s-est-MC}$/GPa	a	b	$E_{s-est-Ed}$/GPa	$E_{sIII-dec}$/GPa
A1-1	22900	35	0.895	0.964	33	32
A1-2		38			42	42
A1-3		33			31	32
C1-1	22900	42	0.356	1.202	44	43
C1-2		35			35	32
C1-3		38			36	40
M1-1	23300	39	0.569	1.062	37	37
M1-2		39			39	40
M1-3		40			42	41

From the results in **Table 2**, it is clear that for compositions A1 and M1, the E-modulus estimation originating from the measured E_d (Equation (5)) is closer to $E_{sIII-dec}$ than the estimation based on the concrete compressive strength (Equation (4)). For concrete C1, the two equations result in approximately the same E-modulus.

4 DISCUSSION

The compressive strength of concrete A1 is, on average, lower than the compressive strength of concrete C1. This is mainly due to the lower water-to-cement ratio (W/C ratio) of composition C1. The significantly larger amount of hydraulic binder in this composition (paste content of about 50 %) enables a large reduction of the W/C ratio to achieve a preferred plastic consistency of the fresh concrete. The estimation of the concrete's compressive strength using the Schmidt hammer resulted in realistic values close to the cylinder compressive strength for all but sample A1-1, where the estimated compressive strength was very low. However, a possible deterioration of the concrete in the protective cover above the steel reinforcement can result in severely underestimated concrete compressive strength. Besides, we still do not know how the ACR reactions change the concrete's hardness.

The dry consistency of concrete A1 and the associated difficult concrete consolidation during its casting into the bunker most likely resulted in a higher proportion of voids in concrete A1 (**Figure 3 right**) compared to concrete C1. An increased volume of voids leads to a lower concrete density and thus a lower compressive strength. Taking into account the data on the density of dolomite aggregates in Slovenia (2810–2840 kg/m³) and the volume of aggregate grains of about 78 %, we would expect the density of concrete A1 to be around 2450 kg/m³ for optimally consolidated concrete (2 % of entrapped pores). This means that the share of voids in the samples of concrete A1 is at least 5–10 %, with consolidation voids ranging from 3 % to 8 %. We can also conclude that there is an excellent linear correlation between the compressive strength of samples A1 and their density (R^2 = 0.93).

On the other hand, samples of concrete C1 have densities of 2400–2480 kg/m³. For concrete with limestone aggregate (densities of 2660–2760 kg/m³), this is possible only with a high volume of hydraulic binder and excellent concrete consolidation. We estimate that the proportion of consolidation voids in samples C1 does not exceed 2 %.

The higher modulus of elasticity of concrete C1 is also due to the higher strength of hydrated cement paste (HCP) in this composition. The significant difference between the initial and stabilized secant E-modulus is most likely due to the inhomogeneous structure of concrete C1 due to the possible segregation and the influence of the HCP creep during the test. The relatively even more significant difference between the initial and stabilized secant E-modulus in concrete A1 is, in addition to the inhomogeneous composition, a consequence of a greater volume of voids due to the difficult compaction of the

fresh concrete. Also, in concrete A1, concrete creep was detected during the test, resulting in more significant residual deformations than in modern concrete.

However, the inhomogeneity of the A1 concrete structure might also be the result of ACR reactions, which is confirmed by the analysed thin sections (**Figure 2 left**). The course of the ACR reactions in concrete with dolomite aggregate and their effects on the concrete properties have been described earlier.[14]

The difference in dynamic E-moduli between compositions A1 and C1 is significantly smaller than the difference in static E-moduli. For concrete A1, the linear correlation between the concrete's density and its E_d is perfect ($R^2 = 1$), mainly due to the high proportion of dolomite aggregate grains in the concrete, which form a skeleton along which ultrasonic waves propagate faster than through HCP. In concrete C1, the volume of aggregate grains is much lower, and the grains are not in contact, so the value of E_d is significantly influenced by HCP.

A comparison of the properties of historic concretes A1 and C1 with the properties of modern concrete (M1) shows that concrete C1 has, on average, the same compressive strength as well as shear and initial static E-modulus. The difference is in the E_d and stabilized static E-modulus, which is 5 GPa and 7 GPa higher for concrete C1. This can be attributed to the large volume of HCP in concrete C1 and the resulting more extensive creep, which consolidates the binder structure and thus increases the concrete's stiffness. On the other hand, concrete A1 showed, on average, the same stabilized E-modulus at a significantly lower compressive strength and E_d compared to concrete M1.

The Poisson's ratios show significantly higher values for concretes A1 and C1 compared to the concrete M1. While the higher v_d for concrete C1 is expected due to the large HCP volume, for concrete A1, $v_d = 0.3$ is an unexpected result. The increased v_d of concrete A1 might be due to ACR reactions.

The estimation of the stabilised secant E-modulus using the ModelCode 2010 for the bunkers of the Rupnik line requires at least average compressive-strength values. We showed, on drilled cylinders, that the parameter $E_{c0} \cdot \alpha_E$ which represents the effect of the aggregate type, is the same for the dolomite and limestone aggregate used when building the bunkers. The cores enable a more detailed study of the concrete's properties and provide data about the elastic properties E_d, G_d and v_d. The compressive strength f_c and the initial and stabilised secant E-moduli can also be determined if the concrete core length is at least equal to its diameter.

5 CONCLUSIONS

The use of non-invasive and non-destructive testing for the characterisation of historical reinforced concrete structures provides a good general approximation and allows at least a partial understanding of construction technology.

It was established that very different concrete compositions were used to build the bunkers, and the extensive scatter of properties was confirmed for each composition due to inhomogeneity and entrapped air voids of the cast concrete. The average compressive strength of the Schmidt hammer for a given position is an acceptable estimation of the actual concrete's compressive strength without a destructive intervention into the bunker. The parameter $E_{c0} \cdot \alpha_E$ of the ModelCode 2010 equation, determined from the test results, seems to have the same value for all the concrete compositions of the Rupnik line. Therefore, the secant stabilised E-modulus estimate using the average compressive strength of the Schmidt hammer and the ModelCode2010 equation is possible for the bunkers. More exact values of the secant stabilised E-modulus can be obtained from the dynamic E-modulus, but the correlation parameters seem to depend on the concrete's composition. Further studies are needed in the area.

The Poisson's coefficients of the historic concrete compositions are higher than the modern reference concrete. The chemical reactions associated with the dissolution, migration and precipitation of new products, such as those observed in the ACR reaction, might be responsible for the increased v_d in the 80-year-old concrete.

6 REFERENCES

[1] K. Ajlec, B. Balkovec, B. Repe, NEČAKOV ZBORNIK Procesi, teme in dogodki iz 19. in 20. stoletja, 2018
[2] J. E. Kaufmann, H. W. Kaufmann, The Forts and Fortifications of Europe 1815-1945: The Central States: Germany, Austria-Hungry and Czechoslovakia, Pen&Sword Military 2014.
[3] A. Jankovič Potočnik, V.Tonič, M. Perpar, Fortifying Europe's Soft Underbelly: The Rupnik Line, the Vallo Alpino and Other Fortifications of the Ljubljana Gap, CreateSpace Independent Publishing Platform 2012
[4] TU 1404 COST ACTION; Towards the Next Generation of Standards for Service Life of Cement-Based Materials and Structures. RRT+ Main phase of the Extended Round Robin Testing programme for TU1404. Testing Protocols, 2016, 28–30
[5] EN 12504-2:2021 – Testing concrete in structures Non-destructive testing. Determination of rebound number, International Organization for Standardization, Brussels.
[6] EN 12504-4:2021 – Testing concrete in structures Determination of ultrasonic pulse velocity, International Organization for Standardization, Brussels
[7] EN 12504-1:2019 – Testing concrete in structures – Part 1: Cored specimens – Taking, examining and testing in compression, International Organization for Standardization, Brussels

[8] EN 12390-1 – Testing hardened concrete Shape, dimensions and other requirements for specimens and moulds, International Organization for Standardization, Brussels.

[9] M. Klun , V. Bosiljkov, V. B. Bosiljkov, The relation between concrete, mortar and paste scale early age properties, Materials, 6 (**2021**) 14, doi:10.3390/ma14061569

[10] EN 12390-13:2013 – Testing hardened concrete – Part 13: Determination of secant modulus of elasticity in compression, International Organization for Standardization, Brussels

[11] EN 12390-3:2019 – Testing hardened concrete Compressive strength of test specimens, International Organization for Standardization, Brussels

[12] F. Bohar, M. Bebar, J. Prosen, Določitev kriterijev za postopka mikro Deval (SIST EN 1097-1) in zmrzlinska obstojnost zrn (SIST EN 1367-1 in SIST EN 1367-2) za naravne, drobljene in reciklirane agregate za nevezane in vezane (stabilizirane) plasti v voziščni konstrukciji. Rezultati laboratorijskih preiskav, Ljubljana-Polje (**2013**).

[13] Fédération internationale du be´ton. Model code 2010: final draft, International Federation for Structural Concrete (fib) (**2012**)

[14] T. Katayama, How to identify carbonate rock reactions in concrete, Materials Characterization, 53 (**2004**), 85–104, doi: doi:10.1016/j.matchar.2004.07.002